The effects of surface stripping ZnO nanorods with argon bombardment

2015 Nanotechnology 26 415701

(http://iopscience.iop.org/0957-4484/26/41/415701)

OPEN ACCESS
IOP Publishing
Nanotechnology

Nanotechnology **26** (2015) 415701 (5pp)
doi:10.1088/0957-4484/26/41/415701

The effects of surface stripping ZnO nanorods with argon bombardment

Chris J Barnett[1,3], Olga Kryvchenkova[1], Nathan A Smith[2], Liam Kelleher[2], Thierry G G Maffeis[1] and Richard J Cobley[1]

[1] Multidisciplinary Nanotechnology Centre, College of Engineering, Swansea University, Singleton Park, Swansea SA2 8PP, UK
[2] Department of Physics, College of Science, Swansea University, Singleton Park, Swansea SA2 8PP, UK

E-mail: 438468@swansea.ac.uk

Received 16 June 2015, revised 17 August 2015
Accepted for publication 27 August 2015
Published 22 September 2015

Abstract

ZnO nanorods are used in devices including field effects transistors, piezoelectric transducers, optoelectronics and gas sensors. However, for efficient and reproducible device operation and contact behaviour, surface contaminants must be removed or controlled. Here we use low doses of argon bombardment to remove surface contamination and make reproducible lower resistance contacts. Higher doses strip the surface of the nanorods allowing intrinsic surface measurements through a cross section of the material. Photoluminescence finds that the defect distribution is higher at the near-surface, falling away in to the bulk. Contacts to the n-type defect-rich surface are near-Ohmic, whereas stripping away the surface layers allows more rectifying Schottky contacts to be formed. The ability to select the contact type to ZnO nanorods offers a new way to customize device behaviour.

S Online supplementary data available from stacks.iop.org/NANO/26/415701/mmedia

Keywords: ZnO, nanorods, defects, argon bombardment, Ohmic contacts, Schottky contacts

(Some figures may appear in colour only in the online journal)

1. Introduction

Zinc oxide (ZnO) is a metal oxide semiconductor with a direct wide band gap of 3.37 eV and a high exciton binding energy of 60 meV [1]. Its novel properties, including high transparency, a large piezoelectric constant, room temperature ferromagnetism, thermal and mechanical stability and the ability to form numerous nanostructures, have meant that it has attracted much attention in recent years [2].

ZnO nanorods have been used in field effects transistors, piezoelectric transducers, optoelectronic devices and gas sensors [3–5]. For efficient and reproducible device operation surface contaminants must be removed using techniques which include surface passivation, annealing and argon bombardment [6–8]. However, numerous studies have shown that the defect chemistry of ZnO changes after annealing which is known to affect the transport properties [9–11]. Dulub *et al* used argon bombardment to remove surface contaminants from single crystal ZnO and vacuum annealing to repair the surface in order to carry out scanning tunnelling microscopy (STM) [8]. Ra *et al* state that they studied the effects of argon ion bombardment on ZnO nanowires by creating a single nanowire FET; however they appear to have used an argon plasma and observed that the mobility, carrier concentration and conductivity increased after treatment [3]. They also carried out photoluminescence (PL) to assess the changes in the defect chemistry, and concluded the change in conductivity was due to a decrease in the electron trapping species on the surface and an increase in oxygen vacancies.

Other recent studies have assessed the effects of argon plasma as well as hydrogen and oxygen plasmas [4, 12, 13].

[3] Author to whom any correspondence should be addressed.

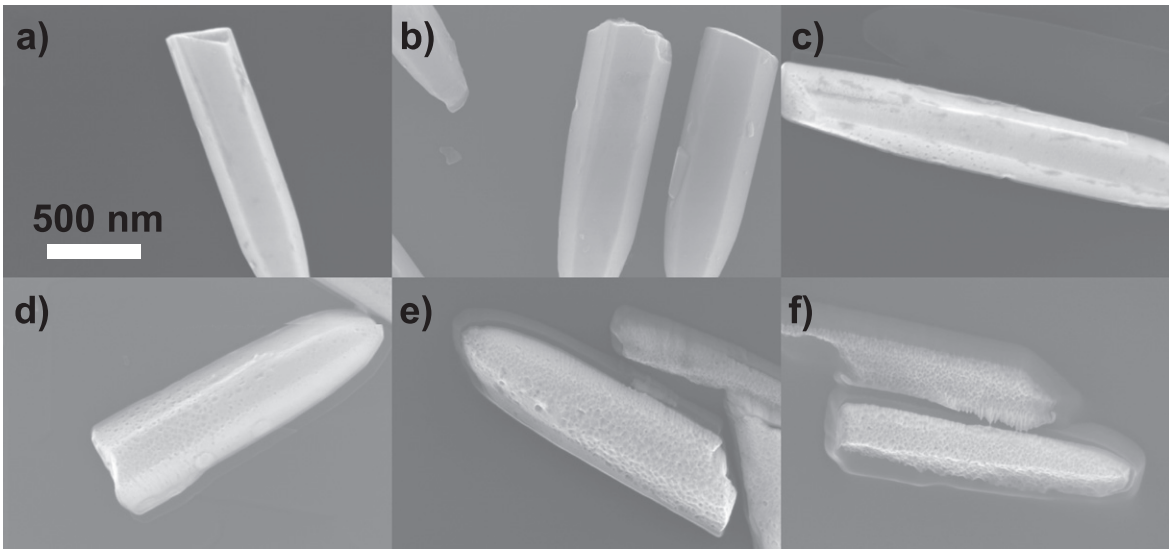

Figure 1. SEM images of ZnO nanorods (a) before; and after 15 min of argon bombardment with dose (b) 2 μA, (c) 12 μA, (d) 19 μA, (e) 23 μA, (f) 26 μA.

Ra *et al* found that oxygen plasma treatment reduced the conductivity by reducing the donor like defect concentration while hydrogen plasma increased the conductivity [12, 13]. Similar effects were seen by Law and Thong who reduced carrier concentration using oxygen plasma [4]. Ionizing argon plasma can cause a substantial negative shift in the threshold gate voltage of a single ZnO nanowire FET while oxygen plasma can cause a substantial positive shift [3, 12].

Here, we use argon bombardment to remove surface contaminants to improve the reproducibility of contact formation. Increased doses have been used to controllably strip the surface of zinc oxide nanorods to investigate the core properties, the distribution of defects and the resulting change in contact formation. Scanning electron microscopy (SEM), nanoscale two point probe, PL and energy dispersive x-ray spectroscopy (EDX) have been used characterize changes in resistance and defect density, with a simulation used to confirm the reason for the changes observed.

2. Experiment

ZnO nanorods were synthesized hydrothermally in a solution of zinc nitrate and hexamine at 90 °C for 9 h and mechanically transferred on to Si/SiO_2 wafers to create two samples (here after referred to as Sample 1 and Sample 2) [14]. Two point probe measurements were carried out on Sample 1 using an Omicron LT Nanoprobe with the tungsten probes annealed to reduce probe oxide contamination [15, 16]. Two tungsten probes were approached onto nanorods using a method developed to ensure minimal compressive strain at the point of contact providing intrinsic characterization [17]. Four *I–V* sweeps were preformed from −1 V to +1 V and averaged on four randomly selected nanorods. For the PL, three spectra were taken from different areas of Sample 2 and averaged. After characterization the nanorods were treated with argon bombardment, using the sample current as a measure of dose, for 15 min. The doses used were 2 μA, 12 μA, 19 μA, 23 μA and 26 μA (which correspond to energies: 0.3 keV, 0.5 keV, 1.0 keV, 1.5 keV and 2 keV) and after each treatment the nanorods were re-characterized, with Sample 1 remaining in vacuum. After the final treatment of argon bombardment Sample 2 was also characterized using EDX.

A 3D simulation with probe diameter 15 nm and probe separation 1100 nm was modelled within Atlas by Silvaco, using a method developed by ourselves, described elsewhere [18, 19]. The material parameters for the ZnO semiconductor used were: bandgap 3.37 eV, electron affinity 4.5 eV, dielectric constant 2.0, conduction band density of states $2.2 \times 10^{18}\,cm^{-3}$, valence band density of $1.8 \times 10^{19}\,cm^{-3}$, and the effective Richardson constants for electrons and holes were $23.7\,A\,cm^{-2}\,K^{-2}$ and $96.3\,A\,cm^{-2}\,K^{-2}$, respectively [20].

Thermionic emission and tunnelling across the Schottky barrier at the probe–nanorod interface were included in the 3D simulations. To calculate thermionic emission current, the surface recombination velocity and the field dependent barrier lowering originating from the image force were taken into account [18, 21]. Tunnelling was considered for both electrons and holes. Using the universal Schottky tunnelling model, the localized tunnelling rates were calculated through the structure of the semiconductor close to the interface [21, 22].

3. Results and discussions

The synthesized nanorods were of hexagonal form with width typically ranging from 250 nm to 350 nm and lengths typically ranging from 1 μm to 2.5 μm. There is no visible difference between the nanorods before argon bombardment (figure 1(a)) and after the 2 μA dose (figure 1(b)). Doses above this caused apparent physical damage to the ZnO nanorods, with a pitted surface and reduced dimensions as a result of bombardment mechanism

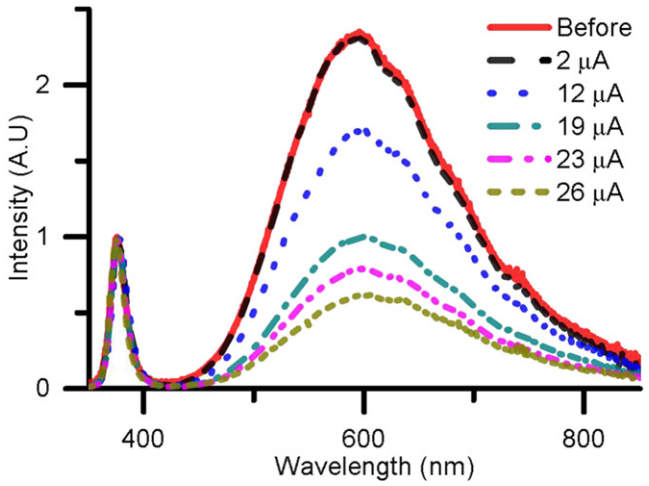

Figure 2. PL spectra for ZnO nanorods with different doses of argon bombardment.

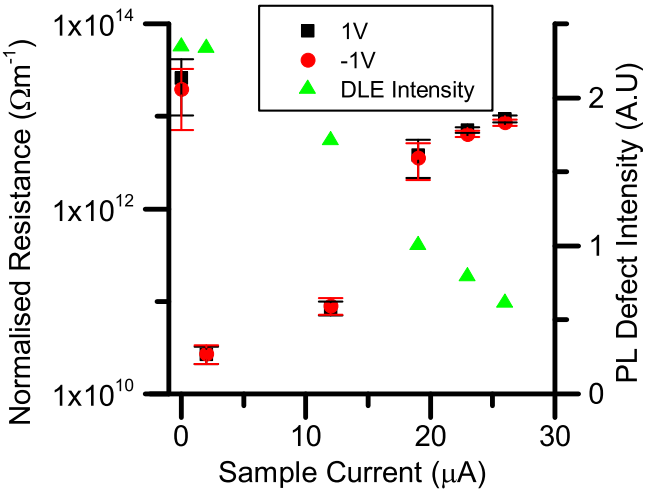

Figure 3. Graph of normalized resistance and DLE peak intensity against the sample current from argon bombardment. Error bars show the standard deviation.

describe by Postawa *et al* [23], seen from figure 1(c) onwards. At higher doses the resulting nanorod is visible within a 'shadow' of same dimensions as the original nanorod. This could be either residual material from the nanorod, or the un-etched silicon substrate protected by the nanorod prior to removal.

High energy ion bombardment can cause argon to be incorporated into the sample which EDX is capable of detecting [24, 25]. However, EDX showed that no argon was present in the ZnO nanorods after argon bombardment at the highest dose.

Damage to nanorods caused by argon bombardment can cause a change in the defect chemistry. Here PL has been used to measure these changes with each spectrum normalized to the near band edge (NBE) peak, presented in figure 2. The NBE peak is centred at 376 nm and the deep level emission (DLE) peak at 595 nm and neither peak changes position after argon bombardment. Fitting of the DLE peak is shown in the supplementary information with four components centred at 543 nm, 595 nm, 638 nm and 765 nm. These defect components are attributed to the following transitions: from the conduction band to an interstitial oxygen defect with no charge O_i [26–29], from an oxygen vacancy with a positive charge V_O^+ to O_i [28, 30, 31], from V_O^+ to an oxygen vacancy defect with no charge V_O [32] and from the conduction band to V_O [29, 33, 34] respectively. The two largest components of the DLE peak are transitions involving the oxygen vacancy with a positive charge. This defect has been identified as the source of the excess electrons causing the n-type nature of ZnO, discussed later. The DLE peak normalized to the NBE peak intensity is plotted in figure 3.

A dose of 2 μA did not significantly change the normalized intensity or shape of the DLE peak. Increased treatment resulted in a drop in the intensity with all component peaks decreasing, which we attribute to the stripping of the nanorod surface. Since the reduction occurs in line with the stripping seen in the SEM images, this implies that these defects are located near the surface of the as grown ZnO nanorods.

Changes in the defect chemistry for ZnO has been shown to alter their electrical transport properties [3]. Here, nanoscale two point-probe was used to perform *I–V* measurements and the mean normalized resistance at +1 V and −1 V is shown against argon bombardment dose in figure 3. Normalized resistance was calculated using the average of the measured resistances of the nanorods divided by the probe separation.

Before argon bombardment the average normalized resistance at +1 V was $2.6 \times 10^{13}\,\Omega\,m^{-1}$ and at −1 V was $2.0 \times 10^{13}\,\Omega\,m^{-1}$ with a large standard deviation suggesting an inconsistent probe-nanorod contact. After a 2 μA dose the normalized resistance decreases to $2.7 \times 10^{10}\,\Omega\,m^{-1}$ at both +1 V and −1 V and the standard deviation reduces. This could be caused by a change in the defect chemistry, although the PL spectra show that there is little to no change in the DLE peak. Therefore, we attribute the drop in normalized resistance to the removal of nanorod surface contamination giving more reproducible lower resistance contacts. Further argon bombardment at higher doses increased the average normalized resistance due to the removal of charge carriers caused by the reduction in the number of oxygen vacancies with a positive charge, as discussed before.

In order to establish the mechanism for the measured change in the electrical behaviour a 3D simulation was developed. A model for two cases was established, firstly for 'cleaned' nanorods, equivalent to the experimental data following the 2 μA argon dose, and secondly for 'etched' nanorods equivalent to the 26 μA treatment. The cleaned nanorods are modelled as a 330 nm diameter wire, with a doping concentration of $10^{18}\,cm^{-3}$, and a surface charge of $5 \times 10^{13}\,cm^{-2}$ to simulate the surface oxygen vacancies identified earlier with PL. For the etched nanorods the diameter is reduced to 270 nm as observed with SEM, the surface charge is removed and the doping concentration is reduced to $10^{16}\,cm^{-3}$ in line with the direction of PL change. For both cases a barrier height of $\varphi_B = 0.27$ eV was used at the metal–nanorod interface.

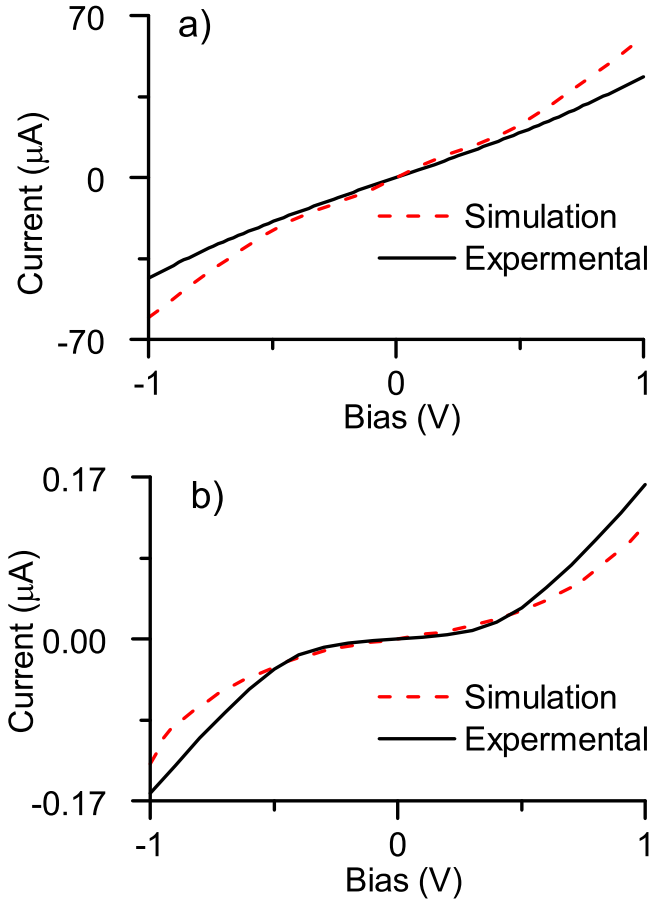

Figure 4. *I–V* characteristics generated using experimental and simulated data for the (a) cleaned and (b) etched nanorods.

In the experimental data Ohmic contacts were formed between the probes and the nanorods both before cleaning and after the first dose, as expected [35]. Measured and simulated *I–V* characteristics of the nanorods are shown in figure 4. For the cleaned case both measured and simulated results indicate primarily an Ohmic contact, which becomes more rectifying after etching. Simulations find that inherent surface charge leads to surface downward band bending before etching. At the contact-nanorod interface the barrier height is pinned and the reduction of the negative surface charge after etching cannot reduce the barrier height, but instead broadens the potential barrier increasing the rectifying response.

Ra *et al* has observed similar results, with a three order of magnitude increase in current after argon plasma treatment, which they attributed to the removal of charge trapping species and increased oxygen vacancies on the surface of their chemical vapour deposition (CVD) grown nanowires [3]. However, their PL results show that the change in the DLE peak is caused by an increase in the number of oxygen vacancies without charge which would not add to the carrier concentration. However we have not observed any charge trapping defects, most likely because CVD grown nanowires have a different defect chemistry with more p-type defects [36]. We suggest it is also possible that Ra *et al* observed increased conductivity due to the removal of surface contaminants with improved contact formation.

There has also been recent discussion that the n-type nature of ZnO is related to hydrogen interstitials rather than oxygen vacancies [28, 37]. These defects would play a similar role by increasing the carrier concentration but cannot be detected using PL. Our results suggest that the defects are concentrated at the near-surface, with oxygen vacancies confirmed as present. Hydrogen interstitials may also be present and play a role, with our results indicating that if so they would be located primarily at the near-surface too.

4. Conclusion

ZnO nanorods have been treated with increasing doses of argon bombardment and the changes in the defect chemistry and electrical transport measured both experimentally and in simulation. A low dose of argon bombardment removed surface contaminants without changing the defect chemistry of the nanorods, resulting in significantly reduced resistance due to improved contact formation.

It has also been found that the defects are located in the near-surface region of the as grown ZnO nanorods. Further argon bombardment at higher doses stripped the surface causing an increase in the measured resistance and a change in the contact nature towards more rectifying. PL results and simulation showed that this is due to the removal of surface charge originating from the n-type defect.

Our work indicates the potential for improving nanorod and nanowire device operation. Firstly, removing surface contaminants with a low dose of argon bombardment gives more reproducible lower resistance contacts without altering the defect chemistry. Secondly, a slightly higher dose can cause pitting of the surface with an increase in the surface area without adversely affecting conductivity. This could see applications in sensing devices such as gas sensors where increased surface area, low resistance materials are highly desirable [38]. Thirdly, selective stripping allows either an Ohmic-like or more Schottky-like contact to the nanorod to be arbitrarily selected. Finally, the technique allows selective probing through the entire nanorod core, potentially allowing other surface sensitive techniques beyond those used here, such as x-ray photoelectron spectroscopy, to be carried out through a cross-section of the material.

Acknowledgments

This work was supported by the EPSRC (grant number EP/J5003181/1).

References

[1] Cheng H, Cheng J, Zhang Y and Wang Q-M 2007 Large-scale fabrication of ZnO micro- and nano-structures by microwave thermal evaporation deposition *J. Cryst. Growth* **299** 34–40
[2] Schmidt-Mende L and MacManus-Driscoll J L 2007 ZnO—nanostructures, defects, and devices *Mater. Today* **10** 40–8

[3] Ra H-W, Choi K S, Ok C W, Jo S Y, Bai K H and Im Y H 2008 Ion bombardment effects on ZnO nanowires during plasma treatment *Appl. Phys. Lett.* **93** 033112

[4] Law J B K and Thong J T L 2008 Improving the NH_3 gas sensitivity of ZnO nanowire sensors by reducing the carrier concentration *Nanotechnology* **19** 205502

[5] Wang X, Song J and Wang Z L 2007 Nanowire and nanobelt arrays of zinc oxide from synthesis to properties and to novel devices *J. Mater. Chem.* **17** 711–20

[6] Lord A M, Maffeis T G, Walton A S, Kepaptsoglou D M, Ramasse Q M, Ward M B, Köble J and Wilks S P 2013 Factors that determine and limit the resistivity of high-quality individual ZnO nanowires *Nanotechnology* **24** 435706

[7] Maffeis T G G, Penny M W, Castaing A, Guy O J and Wilks S P 2012 XPS investigation of vacuum annealed vertically aligned ultralong ZnO nanowires *Surf. Sci.* **606** 99–103

[8] Dulub O, Boatner L A and Diebold U 2002 STM study of the geometric and electronic structure of ZnO(0001)-Zn, (000-1)-O, (10-10), and (11-20) surfaces *Surf. Sci.* **519** 201–17

[9] Tarat A, Nettle C, Bryant D T J, Jones D, Penny M, Brown R, Majitha R, Meissner K and Maffeis T G G 2014 Microwave-assisted synthesis of layered basic zinc acetate nanosheets and their thermal decomposition into nanocrystalline ZnO *Nanoscale Res. Lett.* **9** 11

[10] Ha B, Ham H and Lee C J 2008 Photoluminescence of ZnO nanowires dependent on O2 and Ar annealing *J. Phys. Chem. Solids* **69** 2453–6

[11] Banerjee D, Lao J Y, Wang D Z, Huang J Y, Steeves D, Kimball B and Ren Z F 2004 Synthesis and photoluminescence studies on ZnO nanowires *Nanotechnology* **15** 404

[12] Ra H W, Khan R, Kim J T, Kang B R, Bai K H and Im Y H 2009 Effects of surface modification of the individual ZnO nanowire with oxygen plasma treatment *Mater. Lett.* **63** 2516–9

[13] Ra H-W and Im Y-H 2008 Effect of chemically reactive species on properties of ZnO nanowires exposed to oxygen and hydrogen plasma *Nanotechnology* **19** 485710

[14] Barnett C J, Brown R A, Jones D R, Tarat A, Cobley R J and Maffeis T G G 2012 *Investigation into the Initial Growth Parameters of Hydrothermally Grown Zinc Oxide Nanowires* (20–23 August 2012) pp 1–4

[15] Cobley R J, Brown R A, Barnett C J, Maffeis T G G and Penny M W 2013 Quantitative analysis of annealed scanning probe tips using energy dispersive x-ray spectroscopy *Appl. Phys. Lett.* **102** 023111

[16] Barnett C J, Kryvchenkova O, Wilson L S, Kalna K, Maffeïs T G G and Cobley R J 2015 The role of probe oxide in local surface conductivity measurements *J. Appl. Phys.* **117** 174306

[17] Smith N A, Lord A M, Evans J E, Barnett C J, Cobley R J and Wilks S P 2015 Forming reproducible non-lithographic nanocontacts to assess the effect of contact compressive strain in nanomaterials *Semicond. Sci. Technol.* **30** 065011

[18] Silvaco Inc 2007 ATLAS User's Manual

[19] Lord A M *et al* 2015 Controlling the electrical transport properties of nanocontacts to nanowires *Nano Lett.* **15** 4248–54

[20] Kryvchenkova O, Kalna K and Cobley R J 2014 *Modelling Heating Effects Due to Current Crowding in ZnO Nanowires with End-Bonded Metal Contacts* (20–22 October 2014) pp 1–4

[21] Barnett C J, Kryvchenkova O, Wilson L S J, Maffeis T G G, Kalna K and Cobley R J 2015 The role of probe oxide in local surface conductivity measurements *J. Appl. Phys.* **117** 174306

[22] Kryvchenkova O, Kalna K and Cobley R J 2014 *The Current Crowding Effect in ZnO Nanowires with an End-Bonded Metal Contact* (2–4 July 2014)

[23] Postawa Z, Paruch R, Rzeznik L and Garrison B J 2013 Dynamics of large Ar cluster bombardment of organic solids *Surf. Interface Anal.* **45** 35–8

[24] Lau W M, Bello I, Huang L J, Feng X, Vos M and Mitchell I V 1993 Argon incorporation in Si(100) by ion bombardment at 15–100 eV *J. Appl. Phys.* **74** 7101–6

[25] Oku T and Kuno M 2003 Synthesis, argon/hydrogen storage and magnetic properties of boron nitride nanotubes and nanocapsules *Diam. Relat. Mater.* **12** 840–5

[26] Xu C, Chun J and Kimb D E 2007 Electrical properties and near band edge emission of Bi-doped ZnO nanowires *Appl. Phys. Lett.* **90** 1–3

[27] Yang Y, Yan H, Fu Z, Yang B, Xia L, Xu Y, Zuo J and Li F 2006 Photoluminescence and Raman studies of electrochemically as-grown and annealed ZnO films *Solid State Commun.* **138** 521–5

[28] Lima S A M, Sigoli F A, Jafelicci M Jr and Davolos M R 2001 Luminescent properties and lattice defects correlation on zinc oxide *Int. J. Inorg. Mater.* **3** 749–54

[29] Lin B, Fu Z and Jia Y 2001 Green luminescent center in undoped zinc oxide films deposited on silicon substrates *Appl. Phys. Lett.* **79** 943–5

[30] Liao Z-M, Zhang H-Z, Zhou Y-B, Xu J, Zhang J-M and Yu D-P 2008 Surface effects on photoluminescence of single ZnO nanowires *Phys. Lett.* A **372** 4505–9

[31] Heo Y W, Norton D P and Pearton S J 2005 Origin of green luminescence in ZnO thin film grown by molecular-beam epitaxy *J. Appl. Phys.* **98** 073502

[32] Janotti A and Van de Walle C G 2005 Oxygen vacancies in ZnO *Appl. Phys. Lett.* **87** 122102

[33] Xu P S, Sun Y M, Shi C S, Xu F Q and Pan H B 2003 The electronic structure and spectral properties of ZnO and its defects *Nucl. Instrum. Methods Phys. Res.* B **199** 286–90

[34] Wei X Q, Man B Y, Liu M, Xue C S, Zhuang H Z and Yang C 2007 Blue luminescent centers and microstructural evaluation by XPS and Raman in ZnO thin films annealed in vacuum, N_2 and O_2 *Physica* B **388** 145–52

[35] Lord A M, Ward M B, Evans J E, Davies P R, Smith N A, Maffeis T G and Wilks S P 2014 Enhanced long-path electrical conduction in ZnO nanowire array devices grown via defect-driven nucleation *J. Phys. Chem.* C **118** 21177–84

[36] Smith N A, Evans J E, Jones D R, Lord A M and Wilks S P 2015 Growth of ZnO nanowire arrays directly onto Si via substrate topographical adjustments using both wet chemical and dry etching methods *Mater. Sci. Eng.* B **193** 41–8

[37] Xue X, Wang T, Jiang X, Jiang J, Pan C and Wu Y 2014 Interaction of hydrogen with defects in ZnO nanoparticles—studied by positron annihilation, Raman and photoluminescence spectroscopy *CrystEngCommun.* **16** 1207–16

[38] Jones D R and Maffeïs T G G 2015 Analysis of the kinetics of surface reactions on a zinc oxide nanosheet-based carbon monoxide sensor using an Eley–Rideal model *Sensors Actuators* B **218** 16–24